NEW CLASSIFICATION TECHNIQUES FOR POLARIMETRIC SAR IMAGES AND ASSOCIATED THREE-COMPONENT DECOMPOSITION TECHNIQUE

Yisok Oh, Geba Chang, and Kyung-Yup Lee

Department of Electronics, Information and Communication Engineering, Hongik University, Seoul, Korea
yisokoh@hongik.ac.kr

ABSTRACT: In this paper, we propose one unsupervised classification technique using the degree of polarization (DoP) and the co-polarized phase-difference (CPD) statistics, instead of the entropy and alpha. It is shown that the DoP is closely related to the entropy, and the CPD to the alpha. The DoP explains the feature how much the effect of multiple reflections is contained. Hence, the DoP could be used as an important factor for classifying classes. The CPD can also be computed from the measured Mueller matrix elements. For the smooth surface scattering, the CPD is about 0°, and for dihedral-type scattering, the CPD is about 180°. A DoP-CPD diagram with appropriate boundaries between six different classes is developed based on the SAR image. The classification results are compared with the existing Entropy-alpha diagram as well as the JPL-AirSAR polarimetric data. The technique may have capability to classify an SAR image into six major classes; a bare surface, a village, a crown-layer short vegetation canopy, a trunk-layer short vegetation canopy, a crown-layer forest, and a trunk-dominated forest. Based on the DoP and CPD analysis, a simple three-component decomposition technique was also proposed.

KEY WORDS: Polarimetric SAR images, classification technique, three-component decomposition

1. INTRODUCTION

There are various supervised and unsupervised classification algorithms for polarimetric SAR images. A common unsupervised technique for polarimetric SAR images is the entropy/alpha-based classification technique (Cloude and Pottier, 1997). The entropy/alpha-based technique is to classify the polarimetric response of each pixel into an entropy-alpha diagram, in which the entropy and alpha are computed from Eigen analysis of the covariance matrices. Although the Eigen analysis may be an excellent technique to analyze an information matrix, it has some weak points for the SAR image classification. In the process of the Eigen analysis, the magnitudes of the covariance matrix elements are normalized such that the information in the magnitudes is lost, and consequently it prevents us to proceed to the decomposition process after the Eigen analysis. The existing three-component decomposition technique decomposes the total power into the contributions of single-bounce, double-bounce, and volume scattering terms.

In this paper, we propose one unsupervised classification technique using the degree of polarization (DoP) and the co-polarized phase-difference (CPD) statistics (Ulaby, et al., 1992), instead of the entropy and alpha. It is shown that the DoP is closely related to the entropy, and the CPD to the alpha angle. A DoP-CPD diagram is proposed for classifying any polarimetric SAR image data. The new classification technique is verified with polarimetric AirSAR image data. This classification technique does not include any normalization process for the magnitudes of the covariance matrices. Hence, the DoP-CPD classification technique can be applied to a simple decomposition technique.

2. DEGREE OF POLARIZATION AND CO-POLARIZED PHASE DIFFERENCE

The DoP is defined as the relation of the Stokes parameters, which can be computed from the measured Stokes scattering operator matrix elements. The DoP of a scattered wave provides information on the randomness of the scattering from natural targets (Rio, et al., 2006), because the DoP depends on the effect of multiple reflections.

For full-polarized waves, the scattered electric field is related with the incident wave with the scattering matrix. Then the Stokes vector for the polarized wave is defined as the following relation (Ulaby and Elachi, 1990).

$$\bar{F}^s = \begin{bmatrix} I^s \\ Q^s \\ U^s \\ V^s \end{bmatrix} = \begin{bmatrix} \left\langle \left|E_h^s\right|^2 \right\rangle + \left\langle \left|E_v^s\right|^2 \right\rangle \\ \left\langle \left|E_h^s\right|^2 \right\rangle - \left\langle \left|E_v^s\right|^2 \right\rangle \\ \left\langle 2\,\mathrm{Re}\left(E_h^s E_v^{s*}\right) \right\rangle \\ \left\langle 2\,\mathrm{Im}\left(E_h^s E_v^{s*}\right) \right\rangle \end{bmatrix} \tag{1}$$

The DoP of the polarized wave is defined using the Stokes parameters as in (Ulaby and Elachi, 1990).

$$DoP = \frac{\sqrt{Q^2 + U^2 + V^2}}{I} \tag{2}$$

The received Stokes parameters can be represented with the scattering matrix elements and the incident wave by substituting (1) into (2). Consequently, the Stokes parameters can be expressed as the Stokes scattering

operator matrix elements (or the Mueller matrix elements) using the definition of the Stokes scattering operator matrix in (Zebker and Van Zyl, 1991). For an *h*-polarized wave incidence, the received Stokes vectors are expressed as

$$\begin{aligned} I_h^s &= (M_{11}+M_{22}+2M_{12})+(M_{33}+M_{44}) \\ Q_h^s &= (M_{11}+M_{22}+2M_{12})-(M_{33}+M_{44}), \\ U_h^s &= 2(M_{13}+M_{23}) \\ V_h^s &= -2(M_{14}+M_{24}) \end{aligned} \tag{3}$$

while the received Stokes parameters are expressed in the following relation for a *v*-polarized wave incidence,

$$\begin{aligned} I_v^s &= (M_{11}+M_{22}-2M_{12})+(M_{33}+M_{44}) \\ Q_v^s &= -(M_{11}+M_{22}-2M_{12})+(M_{33}+M_{44}) \\ U_v^s &= 2(M_{13}-M_{23}) \\ V_v^s &= -2(M_{14}-M_{24}) \end{aligned} \tag{4}$$

In equations (3) and (4), $|E_v^i|^2$, $|E_h^i|^2$, $1/r^2$ are ignored, because those terms do not contribute on the computation of the DoP.

The DoP of a partially polarized wave has the range of 0<DoP < 1, where DoP = 1 for a completely polarized wave and D=0 for a completely unpolarized wave. Since the multiple scattering produces significant decrease of the DoP, multiple reflections can be privileged by the DoP. Therefore, the DoP explains well the feature how much the effect of multiple reflections is contained. Hence, the DoP could be used as an important factor for classifying any polarimetric SAR images.

The CPD is defined as the ensemble average of the phase-difference between the *hh*- and *vv*-polarized scattered waves. The measured scattering matrix by a polarimetric radar system can be represented with five quantities; $|S_{vv}|$, $|S_{hh}|$, $|S_{hv}|$, $\phi_c = \phi_{hh} - \phi_{vv}$, and $\phi_x = \phi_{hv} - \phi_{vv}$.

$$[S] = e^{-j\phi_{vv}} \begin{bmatrix} |S_{hh}|e^{-j\phi_c} & |S_{hv}|e^{-j\phi_x} \\ |S_{hv}|e^{-j\phi_x} & |S_{vv}| \end{bmatrix}. \tag{5}$$

For most natural targets, the cross-polarized phase angle ϕ_x is uniformly distributed over [0, 2 π], and therefore contains less target-specific information. On the other hand, the CPD ϕ_c shows a Gaussian PDF with the standard deviation and the mean values which depend on the target characteristics. Hence, the CPD contains some target-specific information (Ulaby, et al., 1992). For extreme cases, for example, CPD=0° for radar scattering from a flat surface, and CPD=180° for a dihedral-type scattering. Otherwise, the CPD has various values depending on the scattering mechanisms, such as single-bounce scattering, double-bounce scattering and volume scattering. For a distributed target, the CPD is obtained from the Stokes scattering operator matrix (or from the Mueller matrix) as follow;

$$\phi_c = \tan^{-1}\left(\frac{\langle \mathrm{Im}(S_{hh}S_{vv}^*)\rangle}{\langle \mathrm{Re}(S_{hh}S_{vv}^*)\rangle}\right) = \tan^{-1}\left(\frac{-2M_{34}}{M_{33}-M_{44}}\right) \tag{6}$$

3. DATA ANALYSIS OF TPOLARIMETRIC SAR IMAGES

Polarimetric SAR image scenes for several sites in Korea could be obtained from the PACRIM-II campaign using the JPL AirSAR system in September, 2000, at P-, L- and C-bands. Among these polarimetric AirSAR images, we selected an image of a study area near Busan in Korea, because the study area includes many different types of terrains. The polarimetric SAR image, at first, is filtered using the Lee filter for a better accuracy. Then, we selected four different sample areas in the study site; i.e., a bare surface, a short vegetation field, a forest, and a town area. Size of each sample area was selected such that it has more than 1200 pixels.

The DoP and CPD values of each pixel of a sample area are positioned in the DoP-CPD diagram with the vertical axis of the DoP and the horizontal axis of the CPD. A histogram for the DoP distribution and another histogram for the CPD are also attached on the DoP-CPD diagram for a better visual aid. Fig. 1 shows, for example, the DoP-CPD diagram for a village area.

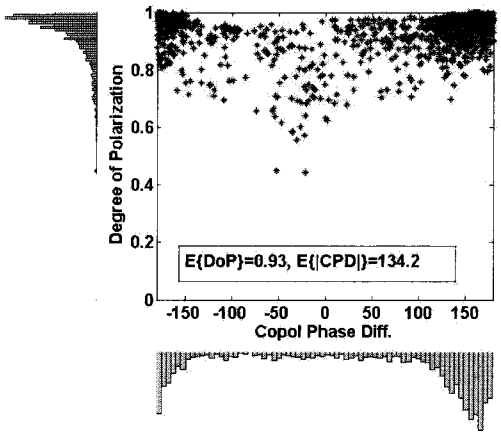

Figure 1. DoP-CPD diagram with histograms for a village area.

Similarly, the DoP-CPD diagrams with histograms for a short vegetation field, a forest, and a town area were generated (refer to Fig. 2 for the DoP-CPD diagram of a short vegetation field).

The PDFs of the DoP and CPD for four different sample areas are compared each other, and the threshold values for classifying SAR image data were determined by checking the cross-over points of the PDF fitting-lines of the different sample areas. The cross-over of the DoP PDF lines between the bare surface and the short vegetation field occurs at DoP=0.85, while the cross-over between the short vegetation field and the forest area at DoP=0.65. The determination of the cross-over value between the single-bounce dominated and the double-bounce dominated backscatter is not obvious. We chose the CPD value of 40^0, comparing the PDF lines of the

CPDs of the short vegetation field (single-bounce dominated) and the forest (mixed with single- and double-bounce scattering mechanism).

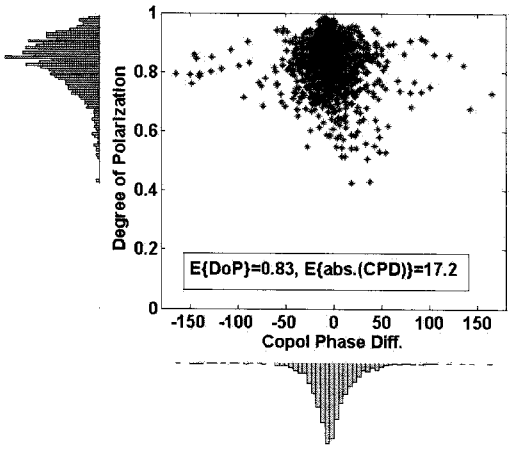

Fig. 2. DoP-CPD diagram with histograms for a short vegetation.

Based on the analysis of the DoP and CPD of the polarimetric image data, a new classification technique with six classification classes is proposed. Fig. 3 shows the DoP-CPD diagram with six different zones. The DoP-CPD diagram can also be used with the absolute values of the CPD so that only half of the DoP-CPD diagram is necessary. Six different zones have their own characteristics as described below.

- Zone I (high-DoP, low-|CPD| backscatter): Physical surfaces such as bare surfaces, water surfaces, sea-ice surfaces will fall in this category.
- Zone II (high-DoP, high-|CPD| backscatter): This zone corresponds to surface scattering with double bounce scattering events. Double-bounce-scattering structures on a bare surface such as a town or village with buildings will fall in this zone.
- Zone III (medium-DoP, low-|CPD| backscatter): The decreased DoP is due to a central statistical distribution of orientation angles of scattering particles. Such a zone would include scattering from relatively short-vegetated fields, such as farming fields.
- Zone IV (medium-DoP, high-|CPD| backscatter): This zone accounts for dihedral scattering with moderate DoP. This may occur with double-bounce backscatters beneath a sparse crown layer with randomly oriented leaves and branches.
- Zone V (low DoP, low-|CPD| backscatter): Volume scattering from a cloud of scatter particles is assumed to arise with DoP<0.65. This zone may include single-bounce dominated deciduous forests or a dense short vegetation fields.
- Zone VI (low DoP, high-|CPD| backscatter): Coniferous forest may have double-bounce scattering at a trunk layer with random scattering through a sparse crown layer, even though this scattering mechanism will depend on frequency.

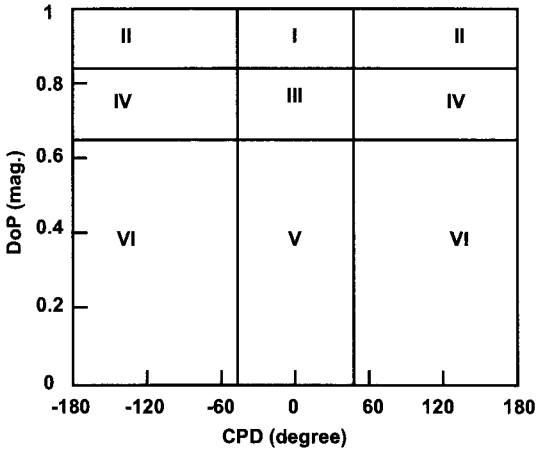

Fig. 3. Six zones of the DoP-CPD diagram

4. VERIFICATION WITH SAR IMAGE DATA

The DoP-CPD diagrams are compared with the entropy-alpha diagram for the selected study areas. Fig. 4 (a) shows the DoP-CPD diagram for the bare surface, while the Fig. 4 (b) shows the entropy-alpha diagram. The number of the pixels for a certain DoP and CPD combination is presented with colors; for example, a red colored point represents for more than 100 pixels at the DoP-CPD position. Most pixels (1155 pixels among 1200 pixels; 96.3 %) of the bare surface are classified to the 'Zone I' of the DoP-CPD diagram as shown in Fig. 4 (a), while the corresponding pixels are positioned in Z9 and Z6 of the entropy-alpha diagram as shown in Fig. 4(b).

Figs. 5 (a) and (b) show the DoP-CPD diagram and the entropy-alpha diagram for a town area of the study site. Most pixels (84.5%) of the town are classified to the 'Zone II' of the DoP-CPD diagram as shown in Fig. 5 (a). For the short vegetation fields, the most pixels (88.6%) are classified to Zone I (28.0%) and Zone II (60.6), because the field is an orchard field with a very sparse tree-canopy.

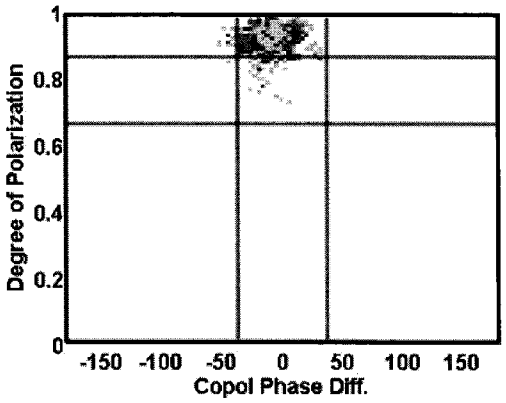

Fig. 4. DoP-CPD diagram for a bare surface.

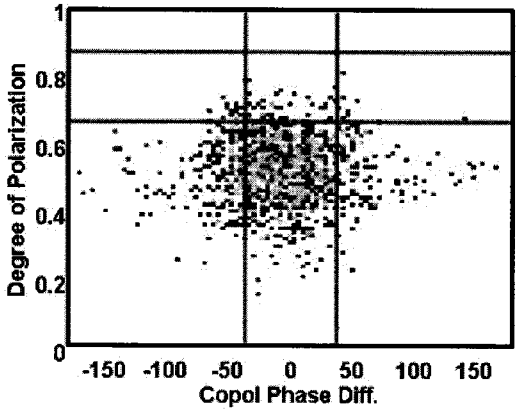

Figure 5 . DoP-CPD diagram for a forest.

For the forest area with tall trees, most pixels (88.8%) are positioned in the Zone V (65.0%) and the Zone VI (23.8%) in the DoP-CPD diagram as shown in Table 1.

Table 1. Accuracy of the classification technique.

Zone	Bare surface		Village		Short veg.		Tall veg.	
	N	%	N	%	N	%	N	%
I	**1153**	**96.3**	44	3.7	336	28.0	0	0.0
II	33	2.8	35	2.9	**727**	**60.6**	97	8.1
III	0	0.0	95	7.9	76	6.3	37	3.1
IV	0	0.0	9	0.8	35	2.9	**780**	**65.0**
V	0	0.0	3	0.3	7	0.6	286	23.8
VI	12	1.0	**1014**	**84.5**	19	1.6	0	0.0
Total	1200	100	1200	100	1200	100	1200	100

Using the analysis of the DoP and the CPD, we can propose a simple three-component decomposition technique with empirically determined threshold values. For example, the volume scattering component may be determined by multiplying (1-DoP) to the total power, and the single- and double-bounce scattering power terms can be separated using the CPD as follows:

$$\begin{aligned} P_v &= P_t \cdot (1 - DoP) \\ P_d &= P_t \cdot DoP \cdot |\phi_c| / 180 \\ P_s &= P_t \cdot DoP \cdot |180 - \phi_c| / 180 \end{aligned} \quad (7)$$

where $P_t = P_s + P_d + P_v$.

Fig. 7 shows the decomposition technique applied to the San Francisco polarimetric SAR image.

5. CONCLUSIONS

Based on the analysis for the DoP and CPD for various earth terrains using polarimetric SAR data, a new SAR image classification technique was proposed, which assigns each image pixel to the six different classes of the DoP-CPD diagram. The accuracy of the new classification technique was examined with polarimetric AirSAR image data, and its results were compared with the existing entropy-alpha classification technique.

Based on the DoP and CPD analysis, a simple three-component decomposition technique was also proposed. It should be noted that the new classification and decomposition techniques were developed with limited sources of polarimetric SAR images, and therefore, these techniques should be examined with more data sets at different frequencies.

Figure 7. Image decomposition technique of this study for the San Francisco area SAR image; green: volume scattering, red: double-bounce scattering, and blue: surface scattering

ACKNOWLEDGEMENTS

This work was supported by the Agency for Defense Development through the Radio-wave Detection Research Center in KAIST.

REFERENCES

Cloude, S. R. and Pottier, E., 1997. An entropy based classification scheme for land applications of polarimetric SAR. *IEEE Trans. Geosci. Remote Sensing*, 35(1), pp. 68-78.

Rio, V. S., Mosquera, J. M., Isasa, M. V., and Lorenzo, M. E., 2006. Statistics of the degree of polarization. *IEEE Trans. Antennas Propag.*, 54,(7).

Ulaby, F. T. and Elachi, C., 1990. *Radar Polarimetry for Geoscience Applications*, Artech House Remote Sensing Library.

Ulaby, F.T., Sarabandi, K., and Nashashibi, A., 1992. Statistical properties of the Mueller matrix of distributed targets. *IEE Proceedings -F*, 139(2), pp. 136-146.

Zebker, H. A. and Van Zyl, J. J., 1991. Imaging radar polarimetry: A review. *Proc. IEEE*, 79(11), pp. 1583-1606.